Extreme Mechanics Letters 29 (2019) 100457

Contents lists available at ScienceDirect

Extreme Mechanics Letters

journal homepage: www.elsevier.com/locate/eml

Crack tip stress based kinetic fracture model of a PVA dual-crosslink hydrogel

Mincong Liu, Jingyi Guo, Chung-Yuen Hui, Alan Zehnder *

Field of Theoretical and Applied Mechanics, Sibley School of Mechanical and Aerospace Engineering, Cornell University, Ithaca NY 14853, United States

ARTICLE INFO

Article history:
Received 22 February 2019
Received in revised form 2 April 2019
Accepted 2 April 2019
Available online 8 April 2019

Keywords:
Creep
Delayed fracture
Viscoelasticity
Large deformation
Failure criterion
Experiment
Finite element

ABSTRACT

The Mode I fracture of a dual-crosslink hydrogel under creep and constant stretch rate loading is investigated experimentally. The hydrogel network contains both permanent, or chemical, bonds and transient, or physical bonds that are constantly breaking and reforming. The resulting material is highly viscoelastic and capable of deforming to large strains prior to failure. Finite element and asymptotic analyses of the crack tip stress fields are used to calculate a stress intensity factor like crack tip parameter. Using this parameter in a kinetic model of failure in which the rate of bond breaking depends exponentially on the stress level, results from creep fracture tests are used to develop a fracture criterion that is then applied to predict failure under constant stretch rate loading conditions.

1. Introduction

A hydrogel is a three-dimensional water-containing polymer network. Hydrogels have been proposed for a number of biomedical applications, such as artificial cartilage [1] and as vehicles for drug delivery [2]. However, conventional hydrogels are too brittle to be used for load carrying applications. Such limitations stimulated the development of mechanically tough hydrogels [3,4]. For instance, Gong et al. were able to synthesize tough hydrogels utilizing the idea of double networks [3]. The first network serves as a sacrificial network: it breaks under load and dissipates energy. The second network is highly extensible, which prevents the growth of macrocracks. One limitation of such hydrogels is that the damage in the sacrificial network is not reversible. To overcome this, researchers have recently introduced noncovalent, transient crosslinks to the second network [5,6]. The transient crosslinks can break and reform during mechanical loading. Breaking of the crosslinks allows the dissipation of energy, and hence increases toughness. Yet the hydrogel can recover to its original state after unloading due to reforming of the transient crosslinks.

To facilitate applications of hydrogels, their mechanical response needs to be better understood and modeled. One important aspect is fracture. Baumberger et al. [7] studied the rate dependent fracture energy in alginate and gelatin hydrogels. They reported that thermally activated "unzipping" of the noncovalent cross-link zones results in slow crack propagation, prevailing against the toughening effect of viscous solvent drag during chain pull-out. Mayumi et al. [8] performed experiments on Poly (vinyl alcohol) hydrogels with a single edge notch. The researchers provided a method to separate the energy dissipated during unloading from that dissipated during crack propagation. Karobi et al. [9] studied creep rupture of Polyampholyte (PA) hydrogels. They found that the introduction of chemical crosslinks in addition to the physical crosslinks modifies the material's resistance to creep flow. Sun et al. [10] studied the fracture of a tough and self-healing PA hydrogel. They proposed that the tearing energy of the PA hydrogel is dominated by the bulk viscoelastic energy dissipation in front of the crack tip. Mishra et al. [11] investigated the fracture of a thermoplastic elastomer gel. They found that these gels fail by a thermally activated process. The energy release rate required to propagate a crack is found to be a function of crack-tip velocity. Recently, the fatigue crack growth of different types of hydrogels was systematically studied by Tang et al. [12], Bai et al. [13,14] and W. Zhang et al. [15] and N. Zhang et al. [16].

Predicting the fracture of novel hydrogels containing transient crosslinks and exhibiting complicated, rate-dependent behavior remains a challenge. Two of the major aspects of understanding fracture in such materials are the crack tip stress and deformation fields and the physics of bond failure. Details of the crack tip fields are complicated by the rate-dependent material behavior and large deformation at the crack tip. Numerical simulations are required to quantitatively study the crack tip fields. Applying

* Corresponding author.
E-mail address: atz2@cornell.edu (A. Zehnder).

https://doi.org/10.1016/j.eml.2019.100457
2352-4316/

the complex constitutive models in numerical simulations poses further challenges [17]. In addition, a fracture criterion applicable to a broad range of hydrogels under different loading conditions is not yet available. While several researchers have been able to adopt models such as that developed Lake and Thomas [18] to explain the fracture behavior of gels and to obtain a measure of fracture toughness [4,8,12,19,20], the complexity of the localized stress near the crack tip has not yet been fully addressed. In order to use a crack tip stress based method to predict the failure of a cracked component, a failure criterion that relates the crack tip fields to the onset of fracture is necessary.

In this work, we study the Mode I fracture of a Poly (vinyl alcohol) (PVA) dual-crosslink hydrogel. The PVA polymer chains are cross-linked by both permanent (covalent) bonds and transient (physical) bonds. The covalent bonds remain attached during loading while the physical bonds can break and reform which results in rate-dependent response of the material. In prior work, we have developed a constitutive model that accurately captures the response of this material under different temperatures and loading rates [21–23]. We have also developed a numerical scheme that allows the application of our constitutive model in a finite element analysis allowing us to simulate the deformation of a specimen with any geometry under any loading [17,24]. However, the constitutive model does not address the final failure of the gel where the covalent chemical bonds fail.

Thus, in this study, we utilize both experimental and numerical tools to study the Mode I fracture of a PVA dual-crosslink hydrogel. The goal of this study is to develop a predictive failure criterion for such materials. The hydrogel specimens are loaded to failure under both constant nominal stress (creep) and constant stretch rate loading conditions. The experiments are simulated using finite element analysis using a constitutive model of the gel developed in previous work. The stress fields near the crack tip are analyzed, providing a means to interpret the experimental results. Based on the interpretation of the experimental results, we propose that a thermally activated failure criterion be adopted to predict failure of the hydrogel.

Such models have their origin in the work of Tobolsky and Eyring [25] who modeled creep rupture failure of polymer threads. In their model bond breaking is assumed to be thermally activated with the breaking rate proportional to $\exp[f\lambda/2NkT]$, where f is the stress on a thread, λ is a length scale, N is the number of bonds per area, T is temperature and k is Boltzmann's constant. Coleman [26] expanded on this model to study the strength distribution of fibers. The model is able to accurately predict the time to failure under constant stress loading (creep rupture) and the distribution of strength in constant stress rate tests. Zhurkov and Korsukov [27] proposed a similar approach and elucidated the physics behind these models. Reviews of these kinetic failure models are given by Henderson et al. [28] and Vanel et al. [29]. In this paper we will adapt the approach of Hansen and Baker [30].

2. Experiment

2.1. Material preparation

The PVA dual-crosslink hydrogels were prepared by incorporating borate ions in a chemically cross-linked PVA gel. Details of synthesis are given in [31]. Here we briefly summarize the procedure. We first made a chemically cross-linked gel by mixing glutaraldehyde solution into PVA solution at pH = 1.4. The PVA concentration in the solution was 12% and the molar ratio of chemical cross linker to PVA monomers was 1:500. The solution was then injected into a mold. After 24 h, the chemically cross-linked gel was removed from the mold and washed with plenty of water to neutralize the pH. Then the chemical gel was soaked in a NaCl/Borax solution (Borax, 1mM/L; NaCl 90 mM/L) for 3 days. The infusion of the ionic solution causes the physical bonds to form.

2.2. Tensile tester

We built a small-scale tensile tester to perform the Mode I fracture tests on the hydrogel specimen. The setup is shown in Fig. 1(a). The specimen was held between two aluminum grips as shown in Fig. 1(b). Sand paper was glued to the inside of the grips to prevent slippage of the specimen. The specimen was immersed in mineral oil during the test to prevent drying. The oil exerts a buoyant force on the grips. This force was calibrated experimentally and subtracted from the measured load to avoid systematic error. Translational motion of the top grip was provided by a Zaber X-LSM200A-E03 translational stage. The load was measured by an Interface SMT1-1.1 load cell (5 N capacity) and the displacement was measured by an OMEGA LD620 LVDT. The load and displacement signals were recorded using a Keithley Model 2701 multiplexing digital voltmeter. The test system was controlled via a MATLAB script incorporating a PID control scheme to hold the load constant during creep fracture tests.

2.3. Mode I fracture tests

We performed Mode I fracture tests on hydrogel specimens under two types of loading conditions: constant nominal stress (creep) and constant stretch rate. The specimen was 12 mm in width, 2 mm in thickness, and 28 mm in gauge length (the length between two grips). A 4 mm edge crack was cut using a razor blade. A sketch of the specimen dimensions is shown in Fig. 1(c).

For the constant nominal stress tests, the specimen was loaded and held under a constant force, until catastrophic fracture occurs. Here the nominal stress, p, is defined as the applied force, P, divided by the uncracked cross-sectional area, A_0(12 mm $\times$ 2 mm). Five different nominal stress levels were applied: 2.80, 3.40, 4.00, 4.75 and 5.50 kPa. For each load level, the tests were repeated three or four times.

For the constant stretch rate tests, specimens were loaded to failure under different constant stretch rates $\dot{\lambda}$. Here the stretch rate, $\dot{\lambda}$, is defined as the change of gauge length per unit time, $\dot{l}$, divided by the original gauge length l_0, i.e., $\dot{\lambda} = \dot{l}/l_0$. The specimens were loaded to failure under four different stretch rates, 0.0003/s, 0.001/s, 0.003/s and 0.01/s. For each stretch rate, the tests were repeated three or four times.

3. Finite element calculation of crack tip fields

To apply the kinetic failure model, the state of stress at the crack tip must be known. Finite element analysis (FEA) is used to calculate the amplitude of the singular crack tip stress fields. The constitutive model used in the FEA is based on a model for the dynamic formation and breaking of the transient bonds in the gel [21,22]. The total strain energy of the PVA gel is the sum of the strain energies carried by the chains connected by chemical and physical crosslinks. The chemical crosslinks do not break; the physical crosslinks can break and heal independently of the loading condition. The breaking and healing kinetics reach dynamic equilibrium. A physical crosslink reforms at zero stress and loses all its strain energy immediately after it breaks. So, its strain energy is characterized by its deformation from the time of reformation to the current time. This constitutive model is completely determined by four independent material parameters, which are fit using data from a relaxation test. The material

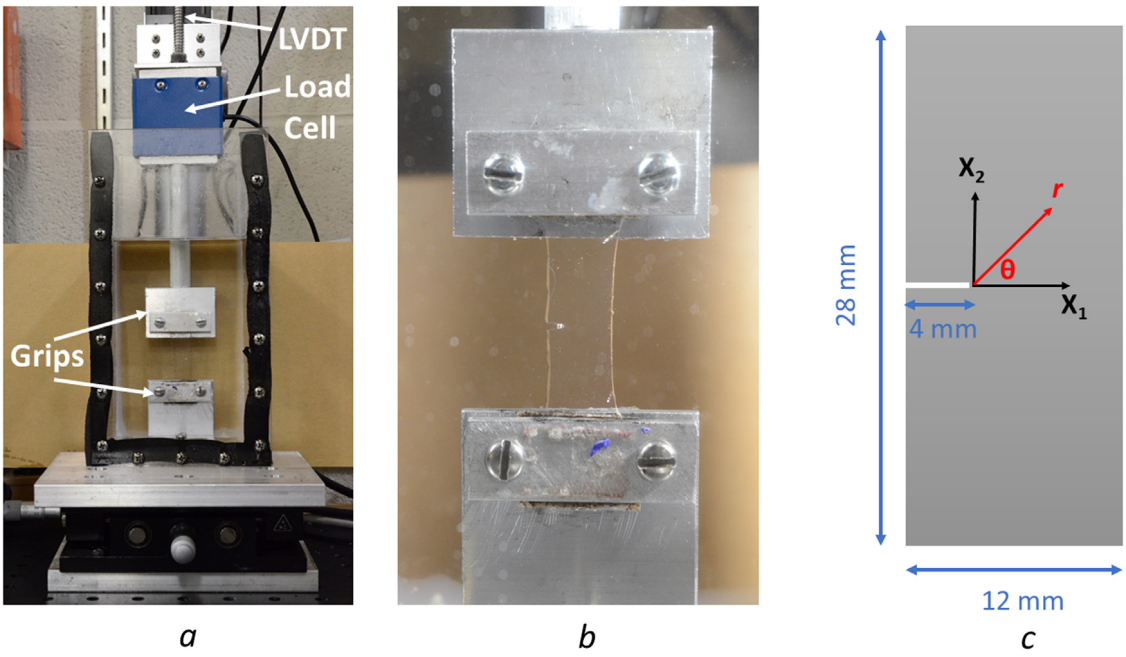

Fig. 1. The custom-built tensile tester and the specimen: (a) overview of the whole system (b) a close-up view of the specimen between two grips (c) the dimensions of the specimen.

parameters used in the simulation are listed in the supplementary information (SI).

We implemented this constitutive model as a user material (UMAT) in ABAQUS with the fitted material parameters. Testing the prediction of the 3D and plane-stress UMATs against experiments, we find that the calculated displacement and stress fields agree well with our asymptotic analysis, and that the crack opening profiles and strain fields compare well with experimental data [17,24].

As discussed in [17], plane stress assumptions work well with thin sheet samples, thus we use the plane stress UMAT in all simulations. Mesh convergence is checked by comparing calculations using a neo-Hookean material model against the asymptotic crack tip fields of a neo-Hookean solid. All simulations are carried out using quadratic plane stress elements. In order to capture the singular stress field near the crack tip, the mesh is highly refined, with a smallest element size of 0.0002 mm.

From the FEM results we extract the logarithmic strain tensor $\boldsymbol{\varepsilon}^{\mathrm{L}}$ and Cauchy stress in front of the crack. We calculate the nominal (PK-I) stresses by

$$\boldsymbol{\sigma} = \boldsymbol{\tau}\mathbf{F}^{-\mathrm{T}}, \text{ where } \mathbf{F} = \mathbf{VR} = \mathbf{V} = \exp\left(\boldsymbol{\varepsilon}^{\mathrm{L}}\right) + \mathbf{I}, \tag{1}$$

where $\mathbf{F}$ is the deformation gradient, $\mathbf{V}$ and $\mathbf{R}$ are the left stretch tensor and rotation tensor, respectively. Because X_1 and X_2 are the principal directions along the crack face, $\mathbf{R} = \mathbf{I}$, the identity tensor. The far field stress, p, is calculated by the total X_2 component of force acting on the top surface, P, divided by the width of the specimen. The total force P is obtained by constraining all nodes on the top surface to one reference point and extracting the reaction force on that reference point. In constant nominal stress simulations, a constant load, P, is applied as the boundary condition. In the constant stretch rate simulations, the displacement on the top surface, which is linearly increasing with time, is prescribed as the boundary condition.

4. Results

4.1. Experimental results

The stress vs. stretch curves up to the point of fracture, for edge cracked samples under constant stretch rates are shown in Fig. 2(a). The PVA dual-crosslink hydrogel clearly shows rate-dependent behavior; it is stiffer as the loading rate increases. This rate dependence results from the breaking and reforming of the physical crosslinks. The hydrogel fractured at different nominal stresses and stretches depending on the stretch rates. The higher the stretch rate, the smaller the stretch ratio at which the specimen fractured. We observe that once crack growth initiates from the tip of the existing crack it propagates rapidly ($\approx$ 100 mm/s), causing complete failure in less than 0.1 s.

The results for the constant stress tests are shown in Fig. 2(b). As creep occurs the stretch increases with time. This behavior is due to the breaking and reforming of the physical crosslinks. When a physical crosslink breaks, the polymer chain that attaches to it is relaxed and it does not carry any stress. Due to this relaxation mechanism, the specimen stretches even while the nominal stress is held constant.

For all the nominal stress levels tested in this study, the failure time vs. applied nominal stress is plotted in Fig. 3. The variations in measured time to failure at each load level are likely due to variations in the crack tip shape of the pre-cut crack. Such dispersion in failure load is also observed in the creep fracture tests of other polymers [30] and indeed arises in many fracture experiments.

It can be seen that the log of t_f, the time to failure, is approximately linear with the applied nominal stress. This indicates that the failure time and the nominal stress follow an exponential relation. Similar behavior was also observed by Karobi et al. in the fracture of Polyampholyte (PA) hydrogels under tensile loading [9] and by Skrzeszewska when loading a TR_4T gel under shear [32]. This exponential relation between fracture time and applied stress suggests that the experimental results can be explained by a thermally activated fracture model.

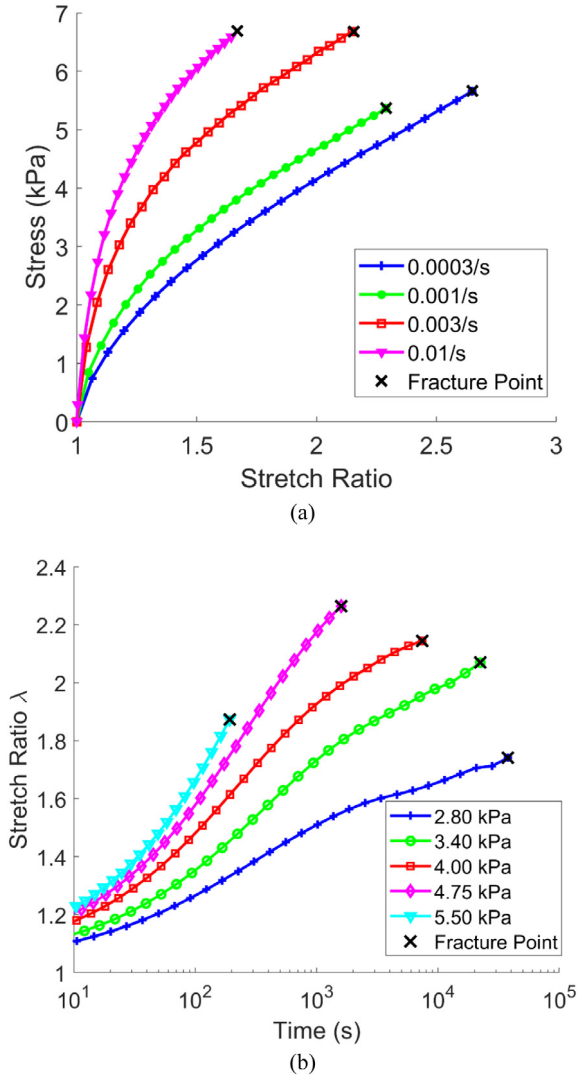

Fig. 2. Experimental results for edge cracked PVA hydrogel specimens: (a) Stress vs. stretch under constant stretch rates. (b) Stretch vs. time under constant applied nominal stress. Each curve represents the average of 3 or 4 tests.

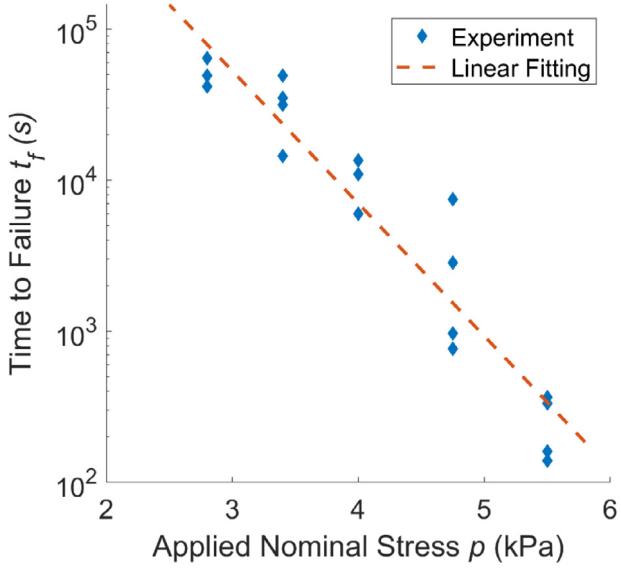

Fig. 3. The time to failure for different stress levels in the constant stress (creep) tests.

4.2. Finite element results

As a first check of the accuracy of the FEM simulations we compared the predicted and measured stretch vs. time in the creep fracture experiments and stress vs. stretch in the constant stretch rate fracture experiments. The finite element results agreed closely with the experimental data, see details of the comparison in the SI.

After validation of the simulations against the overall experimental results, we investigated the stress fields near the crack tip. For our constitutive model, all the chains are assumed to be Gaussian, and a Neo-Hookean model is used for the underlying strain energy. Based on the asymptotic results from [24,33], the nominal stress (first Piola–Kirchhoff, or PK-I, stress) in the primary loading direction near the crack tip should scale inversely with the square root of the distance to the crack tip, that is

$$\sigma_{22} = \overline{B} r^{-1/2} \tag{2}$$

where r is the distance from the crack tip in the undeformed (reference) configuration and $\overline{B}$ is a scaling factor, denoted here as the stress amplitude.

Here we are interested in the nominal (PK-I) stress for the following reason. When the material is under load, consider a reference area A_0 inside the material subject to a total force of F. Assume that there are N_0 polymer chains penetrating this area, sharing the force F. We assume incompressibility. Under load the area A_0 becomes A in the current configuration. For large stretches this current area A will be quite different than A_0. However, the number of chains penetrating this area should, on average, remain the same. Thus the force F is still shared by the same number of bonds N_0, as in the reference area A_0. In this sense, the change of area is not expected to significantly alter the average load carried by each polymer chain. Thus, we argue here that the nominal (PK-I) stress, which refers back to the reference area, be used in the failure model.

From the simulations of the tests, we extracted the stress values on a line extending from the crack tip on ($\theta = 0, r > 0$) and fit the results to a $r^{-1/2}$ singularity. As Fig. 4 shows, for all the stress levels tested in the creep tests, the FEM results can be accurately fit to the $r^{-1/2}$ singularity in the region very close to the crack tip where the asymptotic field dominates.

The stress amplitudes $\overline{B}$ in the figure were obtained directly from the fitting. Here $\overline{B}$ is similar to the stress intensity factor K_I in Linear Elastic Fracture Mechanics (LEFM). In LEFM, for a given specimen, K_I scales linearly with the far-field applied stress p. In other words, the ratio K_I/p should be a constant for a given specimen in LEFM. For the hydrogel, due to the nonlinear material property and large deformation, we do not expect $\overline{B}$ to scale linearly with the applied nominal stress p. To study how the scaling changes with deformation, the ratio $\overline{B}/p$ was calculated at different stretch levels and is plotted in Fig. 5(a) for all creep and constant stretch rate tests. From Fig. 5(a), the ratio $\overline{B}/p$ is not constant. For a stretch level greater than 1.3, $\overline{B}/p$ increases approximately linearly with the stretch ratio. Note that $\overline{B}/p$ results for stretch ratios smaller than 1.3 are not shown. This is because, at small deformations, the region of dominance of the asymptotic stress field solution is too small for the FE simulation to capture without using computationally costly extremely fine meshing.

For the creep tests, it is also informative to look at the variation of $\overline{B}/p$ with respect to time, as shown in Fig. 5(b). From Fig. 5(b), it can be seen that except for the load level of 5.5 kPa when the specimen fractured at about 300 s, $\overline{B}/p$ varies little for most of the test duration. For those experiments, the time to failure ranges from about 4000 s to about 50,000 s, but the ratio $\overline{B}/p$ after 1000 s is nearly constant. Thus, for those tests the $\overline{B}/p$ ratio can be approximated as constant for the duration of the experiment.

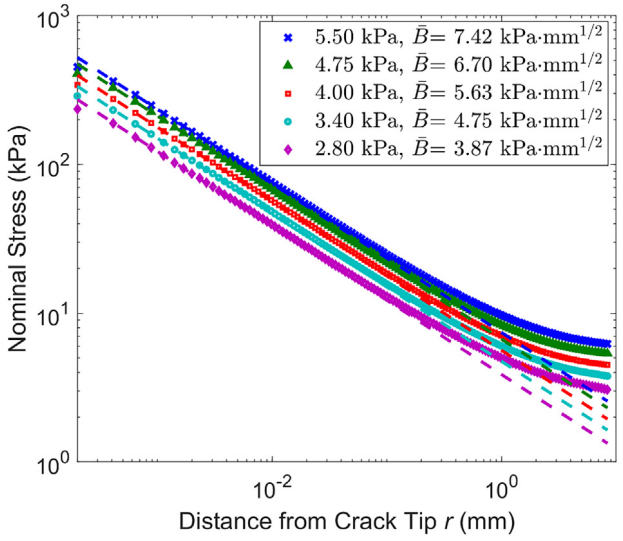

Fig. 4. The nominal stresses for creep tests from finite element simulation and corresponding $r^{-1/2}$ fitting (dashed lines). The nominal stresses are extracted from the time point in the calculation corresponding to when the specimens fail.

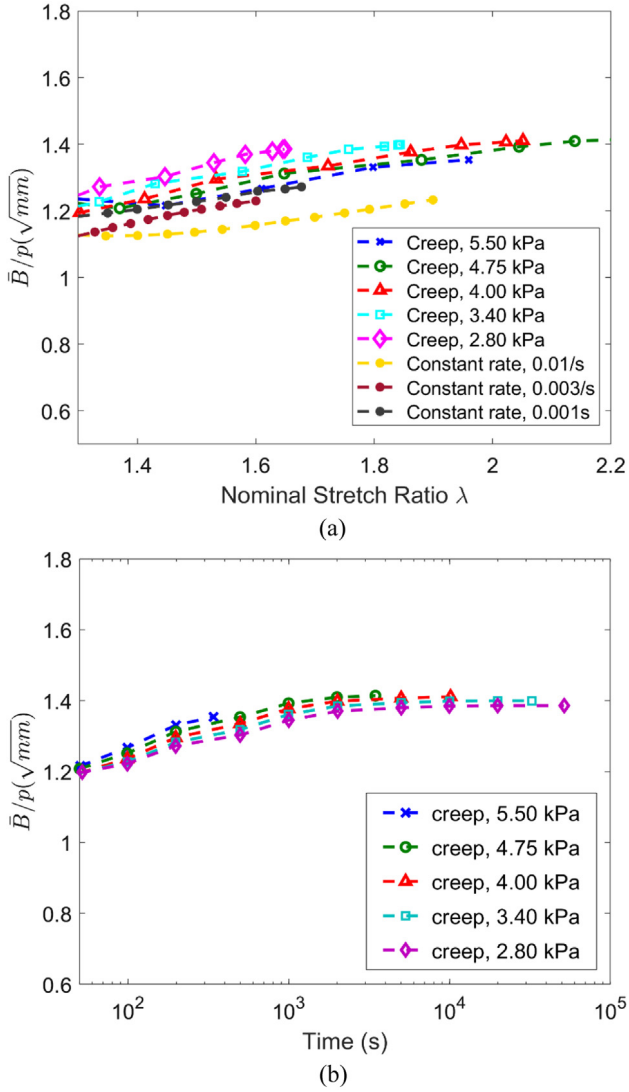

Fig. 5. A close examination of $\bar{B}/p$: (a) The variation of $\bar{B}/p$ with stretch ratio λ for the creep tests and constant rate tests (b) The variation of $\bar{B}/p$ with time for the creep tests.

5. Analysis of creep and constant stretch rate experiments

In uniaxial creep rupture tests of polymers, an exponential relation between the time to failure versus the applied nominal stress is often observed. This suggests a thermally activated fracture process [9,11,32].

The fracture of the PVA hydrogel is due to the breaking of chemical bonds. For a specimen with an edge crack, stress is highly localized near the crack tip and thus the bonds very close to the crack tip will break most rapidly and will nucleate an unstable crack. The breaking of chemical bonds forms a small damage zone near the crack tip. Once there are enough broken bonds in this zone, the material will become unstable and fail instantaneously. This is akin to what Zhurkov and Korsukov argued [27], writing that "*The mechanism of fracture of polymers may be divided into three stages: (1) excitation of bonds under the action of mechanical stress, (2) scission of the excited overstressed bonds by thermal fluctuations, and (3) formation of submicrocracks and their coalescence into larger cracks*".

Under constant stress loading, the time to failure for thermally activated fracture is governed by the classic durability equation [27]:

$$t_f = \tau_0 \exp(\frac{U - \gamma\sigma}{kT}), \tag{3}$$

where t_f is the time to failure, $\tau_0 \approx 10^{-13}$ s is the characteristic oscillation time of atoms in a solid [30,34], U is the activation energy of fracture, γ is a material parameter, characterizing the activation volume of bond rupture, σ is the applied stress, k is the *Boltzmann* constant ($1.38 \times 10^{-23} J\ K^{-1}$), and T is the absolute temperature. Based on this classic theory, Hansen and Baker proposed a rate dependent kinetic theory of fracture for polymers [30] which was able to predict the relation between time to failure and applied stress for PMMA under both constant stress loading and constant stress rate loading. They hypothesized that the total damage accumulation at failure for a given material is, to a good approximation, independent of the mechanical loading condition (stress rate, stress history etc.), which was also experimentally validated in [27]. They proposed a crack damage state variable $n\,(t)$ which characterizes the level of damage (bond breaking). Evolution of the damage state variable, $n\,(t)$ can be written in the form of a differential equation:

$$\frac{dn}{dt} = -K_b n + n_0 K_b,\ n\,(0) = 0 \tag{4}$$

Here $n\,(t) = 0$ corresponds to no damage (initial state). $n\,(t) = 1$ indicates that damage has reached a critical level, resulting in failure of the material under load. The value, $n_0 = 1.58$ is derived by matching the above model to the durability equation (3). K_b is the material breaking rate written as:

$$K_b = \frac{1}{\tau_0} \exp(-\frac{U - \gamma\sigma}{kT}) \tag{5}$$

The differential equation (4) developed by Hansen and Baker expands the applicability of the classic durability equation (3) to cases which have more complex loading history, that is, σ in Eq. (5) need not be constant.

For constant nominal stress tests, Eq. (4) has a closed form solution:

$$\mathrm{n\,(t)} = n_0\,(1 - \exp\,(-K_b t)) \tag{6}$$

Assuming that at the time of failure (t_f), $n\left(t=t_f\right)=1$, Eq. (6) can be written as:

$$\ln t_f = -\frac{\gamma}{kT}\sigma + \frac{U}{kT} + \ln \tau_0 \tag{7}$$

Eq. (7) can also be obtained directly from (3), and can be applied to predict creep failure of uncracked polymer specimens under uniform, constant applied stress.

However, the test specimen in our experiments has an edge crack in it and thus the stress is not uniform, but highly concentrated near the crack tip. To take this into account, we use the crack tip stress. From asymptotic analysis and the finite element simulation, in the region very close to the crack tip, the nominal stress, σ_{22}, in the primary loading direction is singular and can be written as $\sigma_{22} = \overline{B}/\sqrt{r}$, where $\overline{B}$ is the stress amplitude factor similar to the stress intensity factor in linear elastic fracture mechanics. Note that in a region very close to the crack tip, where active bond failure is taking place the stress may deviate from the $1/\sqrt{r}$ singularity if the material response deviates from the neo-Hookean assumption. In prior work [17,35] using the neo-Hookean assumption and neglecting effects of poroelastic flow we were able to obtain a good prediction of the crack opening displacement at a large stretch as well as a good predication of the crack tip strain field, even for Lagrangian strains of over 1000% and to within 0.1 mm from the crack tip. Those results indicate that neo-Hookean without poroelasticity is a reasonable model for this case, or at least that any deviations are below the resolution of our experimental methods.

In place of σ in Eq. (7) we use the crack tip stress value calculated at a distance r_c from the crack tip. Equivalently one can think of this as the stress averaged over a distance r_c from the crack tip. Denoting this stress value as σ_c we have

$$\sigma_c = \frac{\overline{B}}{\sqrt{r_c}}. \tag{8}$$

The distance r_c can be thought of as representing the molecular size scale of bond rupture [36,37] .

With σ in Eq. (7) replaced by σ_c from Eq. (8), for the creep rupture tests the failure time is

$$\ln t_f = -\frac{\gamma}{kT}\frac{\overline{B}}{\sqrt{r_c}} + \frac{U}{kT} + \ln \tau_0. \tag{9}$$

In the previous section, we showed that for the creep tests, the ratio $\overline{B}/p$ for the creep tests did not vary significantly during the tests and that this ratio is almost independent of the applied stress (see Fig. 5(b)). Thus, we approximate $\overline{B}/p$ as a constant,

$$\overline{B}/p = C_B. \tag{10}$$

Here C_B is the scale coefficient which we assume to be constant for all the constant stress (creep) tests. From the results of Fig. 5(b), $C_B \approx 1.4\sqrt{\text{mm}}$ for all creep tests. Substitute (10) into (9) and rearrange the equation to obtain the relation between the time to failure t_f and the applied nominal stress p for a specimen containing a pre-crack

$$\ln t_f = -\frac{\gamma}{kT}\frac{C_B}{\sqrt{r_c}}p + \frac{U}{kT} + \ln \tau_0 \tag{11}$$

From (11), with C_B constant, the log of time to failure, $\ln t_f$, will still be linearly proportional to the applied far-field nominal stress, p, even when a pre-crack exists. This is consistent with what is observed in the experimental results of the creep fracture tests, Fig. 3.

We performed a linear fitting of $\ln t_f$ and p. With the slope and intercept from the fitting, the fitting parameters, which are the activation energy U and $\gamma/\sqrt{r_c}$ can be obtained. Since there is scatter in the measured failure times at each applied stress level, we compute the fitting parameters that lie in the 95% confidence interval, as listed in Table 1.

Table 1
Summary of fracture model parameters from fitting of constant stress tests.

Parameter	Lower bound of 95% confidence interval	Upper bound of 95% confidence interval
U (J)	1.85×10^{-19}	1.97×10^{-19}
$\gamma/\sqrt{r_c}$ ($\text{m}^{5/2}$)	1.54×10^{-22}	2.17×10^{-22}

The above shows that by combining the nominal stress field near the crack tip with a thermally activated failure criterion, we are able to relate the time to failure of the hydrogel specimens under creep tests to the applied nominal stress. To test the applicability of this failure criterion to other situations, we use the model parameters obtained from the creep tests to predict the failure of hydrogel specimens under *constant stretch rate* tests. For the constant stretch rate tests, a closed form solution of (4) is not available thus the model is integrated numerically. Eqs. (4) and (5) can be written in a discrete form, with the crack tip stress taken into account:

$$\frac{n(t_{i+1})-n(t_i)}{\Delta t} = -K_{b_i}n(t_i) + n_0K_{b_i} \tag{12}$$

$$K_{b_i} = \frac{1}{\tau_0}\exp\left(-\frac{U-\frac{\gamma C_B}{\sqrt{r_c}}p_i}{kT}\right) \tag{13}$$

Here the subscript i denotes the ith time step. C_B and $\sqrt{r_c}$ are introduced to take into account the existence of a sharp crack, as discussed before. The material parameters U and $\gamma/\sqrt{r_c}$ were obtained from the constant nominal stress tests and are applied directly to the constant stretch rate tests. The nominal stress history p_i for the constant stretch rate tests are available from the experiments. For the constant stretch rate loading, from Fig. 5(a), C_B scales approximately linearly with the stretch ratio λ. Thus, from the results of Fig. 5(a), for each constant stretch rate test, we performed a linear fit between C_B and λ. In this way C_B at a given stretch ratio can be estimated. We did not perform a finite element simulation for the stretch rate 0.0003/s, but from the trend in Fig. 5(a) it is reasonable approximation that $C_B$vs. λ for 0.0003/s is close to that of the rate 0.001/s.

Now we can integrate Eq. (12) to calculate the evolution of $n\,(t)$. The predicted failure time for the constant stretch rate tests is the time corresponding to $n\,(t)=1$. The predictions of the failure theory are compared with the experimental results in Fig. 6. It can be seen that this failure criterion yields a good overall prediction of fracture under constant stretch rate loading. The agreement between the model prediction and experiments is very close for the loading rates of 0.0003/s, 0.001/s and 0.003/s. The predicted time to failure is slightly too long for 0.01/s. One reason may be that, for the creep tests, the average stretch rates are on the order of 0.0001/s to 0.001/s, which is much slower than the fastest loading rate for the constant stretch rate test, 0.01/s. Thus the failure criterion may have limitations when predicting the failure of specimens at high loading rates.

Previously, we obtained the parameters U and $\gamma/\sqrt{r_c}$. U is the activation energy of bond failure, and is a material dependent quantity. Converting units, the activation energy for the PVA gel is 111 to 118 kJ/mole, close to the values of 117–125 kJ/mole reported by Hansen and Baker [30] for PMMA and 113 to 125 kJ/mole for HDPE, LDPE and PP [37].

The parameter $\gamma/\sqrt{r_c}$ requires some explanation. Here γ is the activation volume and r_c is a distance used to compute the crack tip stresses. We have no means to directly measure γ or r_c. However, one way to interpret these parameters is to relate the activation volume to the distance r_c, i.e. $\gamma \sim r_c^3$ In that

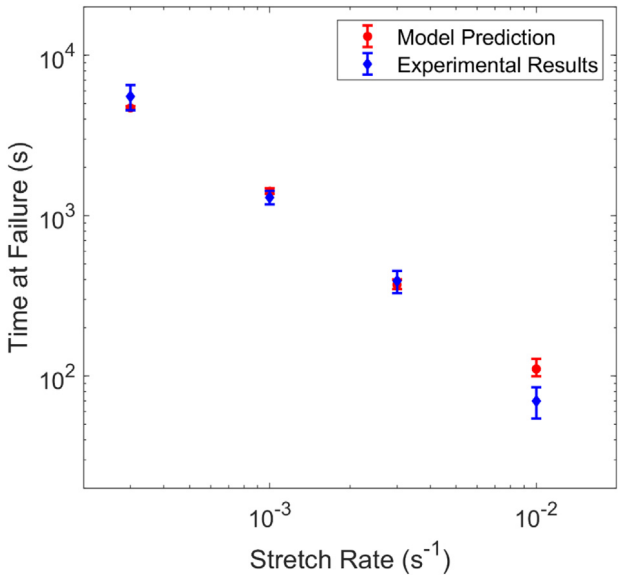

Fig. 6. Comparison between the failure time predicted by the kinetic fracture theory and experimental results at constant stretch rates. For the model predictions, the error bars are based on the 95% confidence interval of the material fitting parameters.

case $\gamma/\sqrt{r_c}$ reduces to $r_c^{2.5}$. Based on our fitting, we deduce a characteristic activation length of $\gamma^{1/3} = 2.1$ nm. This length is comparable to the characteristic activation length of 3 nm Karobi et al. reported for a polyampholyte gel [9]. Reported values of $\gamma^{1/3}$ for dense polymers range from about 0.1 to 17 nm [30,36,37]. The activation volume can be thought of as representing the molecular size scale of bond breaking. Dijkstra [36] states it in words as: "*activation volume* $\approx$ *chain cross-section* $\times$ *bond length perpendicular to the cross-section* $\times$ *elongation at break*".

6. Conclusion

In this study, we utilized experiments and finite element simulations to study the Mode I fracture of a PVA dual-crosslink hydrogel under creep and constant extension rate loadings. The goal of this study is to propose a practical failure criterion for such materials.

From the experimental results, it is shown that for the creep tests, the time to failure and applied stress follow an exponential relationship. For the constant stretch rate tests, the specimens failed at different stresses and stretches for different loading rates. Using a constitutive model and a numerical scheme we developed in our previous work, we obtained the stress fields near the crack tip with finite element simulation. By utilizing a concept of stress at a characteristic distance, we established the connection between the nominal stress amplitude, $\overline{B}$, near the crack tip and the far field applied stress. Combining the nominal stress amplitude and a kinetic bond breaking model, we fit the exponential relation between time to failure and the applied stress levels observed in creep tests. With material parameters obtained from fitting of the creep tests, we are able to accurately predict fracture during constant stretch rate tests using the same failure criterion. Future research could include further testing of the validity of this criterion by applying it under cyclic loading, at varying temperatures and to different hydrogels.

Acknowledgment

This material is based upon work supported by the National Science Foundation under Grant No. CMMI-1537087.

Appendix A. Supplementary data

Supplementary material related to this article can be found online at https://doi.org/10.1016/j.eml.2019.100457.

References

[1] H.J. Kwon, K. Yasuda, J.P. Gong, Y. Ohmiya, Polyelectrolyte hydrogels for replacement and regeneration of biological tissues, Macromol. Res. 22 (3) (2014) 227–235.
[2] Y. Qiu, K. Park, Environment-sensitive hydrogels for drug delivery, Adv. Drug Deliv. Rev. 53 (3) (2001) 321–339.
[3] J.P. Gong, Y. Katsuyama, T. Kurokawa, Y. Osada, Double-network hydrogels with extremely high mechanical strength, Adv. Mater. 15 (14) (2003) 1155–1158.
[4] R.E. Webber, C. Creton, H.R. Brown, J.P. Gong, Large strain hysteresis and mullins effect of tough double-network hydrogels, Macromolecules 40 (8) (2007) 2919–2927.
[5] K.J. Henderson, T.C. Zhou, K.J. Otim, K.R. Shull, Ionically cross-linked triblock copolymer hydrogels with high strength, Macromolecules 43 (14) (2010) 6193–6201.
[6] T.L. Sun, et al., Physical hydrogels composed of polyampholytes demonstrate high toughness and viscoelasticity, Nature Mater. 12 (10) (2013) 932–937.
[7] T. Baumberger, O. Ronsin, From thermally activated to viscosity controlled fracture of biopolymer hydrogels, J. Chem. Phys. 130 (6) (2009) 061102.
[8] K. Mayumi, J. Guo, T. Narita, C.Y. Hui, C. Creton, Fracture of dual crosslink gels with permanent and transient crosslinks, Extreme Mech. Lett. 6 (2016) 52–59.
[9] S.N. Karobi, et al., Creep behavior and delayed fracture of tough polyampholyte hydrogels by tensile test, Macromolecules 49 (15) (2016) 5630–5636.
[10] T.L. Sun, et al., Bulk energy dissipation mechanism for the fracture of tough and self-healing hydrogels, Macromolecules 50 (7) (2017) 2923–2931.
[11] S. Mishra, R.M. Badani Prado, T.E. Lacy, S. Kundu, Investigation of failure behavior of a thermoplastic elastomer gel, Soft Matter 14 (39) (2018) 7958–7969.
[12] J. Tang, J. Li, J.J. Vlassak, Z. Suo, Fatigue fracture of hydrogels, Extreme Mech. Lett. 10 (2017) 24–31.
[13] R. Bai, Q. Yang, J. Tang, X.P. Morelle, J. Vlassak, Z. Suo, Fatigue fracture of tough hydrogels, Extreme Mech. Lett. 15 (2017) 91–96.
[14] R. Bai, J. Yang, X.P. Morelle, C. Yang, Z. Suo, Fatigue fracture of self-recovery hydrogels, ACS Macro Lett. 7 (3) (2018) 312–317.
[15] W. Zhang, et al., Fatigue of double-network hydrogels, Eng. Fract. Mech. 187 (2018) 74–93.
[16] N. Zhang, Z. Pan, J. Lei, Z. Liu, Effects of temperature on the fracture and fatigue damage of temperature sensitive hydrogels, RSC Adv. 8 (54) (2018) 31048–31054.
[17] J. Guo, et al., Fracture mechanics of a self-healing hydrogel with covalent and physical crosslinks: A numerical study, J. Mech. Phys. Solids (2018).
[18] G.J. Lake, A.G. Thomas, The strength of highly elastic materials, Proc. R. Soc. Lond. Ser. A Math. Phys. Eng. Sci. 300 (1460) (1967) 108–119.
[19] J. Cui, M.A. Lackey, G.N. Tew, A.J. Crosby, Mechanical properties of end-linked PEG/PDMS hydrogels, Macromolecules 45 (15) (2012) 6104–6110.
[20] R. Long, C.-Y. Hui, Fracture toughness of hydrogels: measurement and interpretation, Soft Matter 12 (39) (2016) 8069–8086.
[21] R. Long, K. Mayumi, C. Creton, T. Narita, C.-Y. Hui, Time dependent behavior of a dual cross-link self-healing gel: Theory and experiments, Macromolecules 47 (20) (2014) 7243–7250.
[22] J. Guo, R. Long, K. Mayumi, C.-Y. Hui, Mechanics of a dual cross-link gel with dynamic bonds: Steady state kinetics and large deformation effects, Macromolecules 49 (9) (2016) 3497–3507.
[23] M. Liu, J. Guo, C.-Y. Hui, C. Creton, T. Narita, A. Zehnder, Time–temperature equivalence in a PVA dual cross-link self-healing hydrogel, J. Rheol. 62 (4) (2018) 991–1000.
[24] J. Guo, C.Y. Hui, M. Liu, A.T. Zehnder, The stress field near the tip of a plane stress crack in a gel consisting of chemical and physical cross-links, in preparation, Proc. R. Soc. A.
[25] A. Tobolsky, H. Eyring, Mechanical properties of polymeric materials, J. Chem. Phys. 11 (3) (1943) 125–134.
[26] B.D. Coleman, Time dependence of mechanical breakdown phenomena, J. Appl. Phys. 27 (8) (1956) 862–866.
[27] S.N. Zhurkov, V.E. Korsukov, Atomic mechanism of fracture of solid polymers, J. Polym. Sci. Polym. Phys. Ed. 12 (2) (1974) 385–398.
[28] C.B. Henderson, P.H. Graham, C.N. Robinson, A comparison of reaction rate models for the fracture of solids, Int. J Fract. Mech. 6 (1) (1970).
[29] L. Vanel, S. Ciliberto, P.-P. Cortet, S. Santucci, Time-dependent rupture and slow crack growth: elastic and viscoplastic dynamics, J. Phys. Appl. Phys. 42 (21) (2009) 214007.

[30] A.C. Hansen, J. Baker-Jarvis, A rate dependent kinetic theory of fracture for polymers, Int. J. Fract. 44 (3) (1990) 221–231.
[31] K. Mayumi, A. Marcellan, G. Ducouret, C. Creton, T. Narita, Stress–strain relationship of highly stretchable dual cross-link gels: Separability of strain and time effect, ACS Macro Lett. 2 (12) (2013) 1065–1068.
[32] P.J. Skrzeszewska, J. Sprakel, F.A. de Wolf, R. Fokkink, M.A. Cohen Stuart, J. van der Gucht, Fracture and self-healing in a well-defined self-assembled polymer network, Macromolecules 43 (7) (2010) 3542–3548.
[33] R. Long, C.-Y. Hui, Crack tip fields in soft elastic solids subjected to large quasi-static deformation — A review, Extreme Mech. Lett. 4 (2015) 131–155.
[34] S.N. Zhurkov, Kinetic concept of the strength of solids, Int. J. Fract. 26 (4) (1984) 295–307.
[35] M. Liu, J. Guo, C.-Y. Hui, A.T. Zehnder, Application of Digital Image Correlation (DIC) to the Measurement of Strain Concentration of a PVA Dual-Crosslink Hydrogel Under Large Deformation, in preparation, Exp. Mech.
[36] D.J. Dijkstra, J.C.M. Torfs, A.J. Pennings, Temperature-dependent fracture mechanisms in ultra-high strength polyethylene fibers, Colloid Polym. Sci. 267 (10) (1989) 866–875.
[37] H.-H. Kausch, Polymer Fracture, Springer Science & Business Media, 2012.